Chemistry
A European
Journal

Chemistry Europe
European Chemical Societies Publishing

Accepted Article

Title: Intense Photoinduced Intervalence Charge Transfer in High-Valent Iron Mixed Phenolate/Carbene Complexes

Authors: Alejandro Cadranel, Lisa Gravogl, Dominik Munz, and Karsten Meyer

To be cited as: *Chem. Eur. J.* **2022**, e202200269

Link to VoR: https://doi.org/10.1002/chem.202200269

WILEY-VCH

10.1002/chem.202200269

WILEY-VCH

FULL PAPER

Intense Photoinduced Intervalence Charge Transfer in High-Valent Iron Mixed Phenolate/Carbene Complexes

Alejandro Cadranel,*[a],[b],[c] Lisa Gravogl,[d] Dominik Munz,[d],[e] Karsten Meyer[d]

Dedicated to Prof. José A. Olabe on the occasion of his 80th birthday.

[a] Dr. Alejandro Cadranel
Department Chemie und Pharmazie, Physikalische Chemie
Friedrich-Alexander-Universität Erlangen-Nürnberg
Egerlandstraße 3, 91058 Erlangen, Germany
E-mail: ale.cadranel@fau.de
[b] Dr. Alejandro Cadranel
Departamento de Química Inorgánica, Analítica y Química Física
Universidad de Buenos Aires, Facultad de Ciencias Exactas y Naturales
Pabellón 2, Ciudad Universitaria, C1428EHA, Buenos Aires, Argentina.
[c] Dr. Alejandro Cadranel
Instituto de Química Física de Materiales, Medio Ambiente y Energía (INQUIMAE)
CONICET – Universidad de Buenos Aires
Pabellón 2, Ciudad Universitaria, C1428EHA, Buenos Aires, Argentina
[d] Lisa Gravogl, Prof. Dr. Dominik Munz, Prof. Dr. Karsten Meyer
Department Chemie und Pharmazie, Anorganische Chemie
Friedrich-Alexander-Universität Erlangen-Nürnberg
Egerlandstraße 1, 91058 Erlangen, Germany
[e] Prof. Dr. Dominik Munz
Anorganische Chemie: Koordinationschemie
Universität des Saarlandes
Campus C4.1, 66123 Saarbrücken, Germany

Supporting information for this article is given via a link at the end of the document.

Abstract: We report high-valent iron complexes, supported by *N*-heterocyclic carbene (NHC)-anchored, bis-phenolate pincer ligands that undergo ligand-to-metal charge transfer (LMCT) upon photoexcitation. The resulting excited states – with a lifetime in the pico-second range – feature a ligand-based mixed-valence system and intense intervalence charge transfer bands in the near-infrared (NIR) region. Upon oxidation of the complex, corresponding intervalence charge transfer (IVCT) absorptions are also observed in the ground state. We suggest that the spectroscopic hallmarks of such LMCT states provide useful tools to decipher excited state decay mechanisms in high-valent NHC complexes. Our observations further indicate that NHC-anchored, bis-phenolate pincer ligands are not sufficiently strong donors to prevent the population of excited metal-centered (MC) states in high-valent iron complexes.

Introduction

The discovery of energy conversion schemes that are not only efficient and robust, but also cheap, environmentally friendly, and sustainable, is a main target of molecular chemical research. The current state-of-the-art to convert sunlight into electricity or fuels largely makes use of the 4*d* and 5*d* transition metals, which are typically more toxic, expensive, and scarce than their first-row congeners. Apart from the well-established use of the lanthanides,[1] this resulted in the exploration of V,[2,3] Cr,[4–6] Mn,[7] Fe,[8–12] Co,[13] Cu[14–16] and Zr[17] as well as *s*-block complexes [18,19] for the application as emitters[20,21] or components in solar cells.[22–24] Amongst the 3*d* metals mentioned above, iron is particularly attractive due to its abundance, environmental friendliness and low toxicity. Recently, significant progress regarding the prolongation of excited state lifetimes allowed some iron chromophores to compete with model ruthenium or osmium chromophores.[25–28]

One of the leading strategies for the design of iron-based chromophores is the use of strong donor ligands.[29] The resulting large ligand-field splitting destabilizes metal-centered (MC) excited states, whose population is generally detrimental due to their short lifetimes.[30] Further, strongly donating ligands, such as *N*-heterocyclic carbenes (NHCs), are particularly relevant in stabilizing high-valent metal oxidation states, such as iron in oxidation states +IV,[31–33] +V,[34] and +VI,[35] including air- and moisture stable Fe(V) complexes.[36] In consequence, long-lived ligand-to-metal charge transfer (LMCT) states can be obtained in iron-NHC complexes. In fact, many of the most appealing chromophores are based on earth-abundant transition metal complexes and involve high-valent metal ions and LMCT excited states, and some examples of LMCT emitters have been documented.[7,13,37] This contrasts with traditional ruthenium and osmium chromophores, combining metal(II) ions with π-acceptor ligands, leading typically to MLCT excited states. While MLCT excited states have extensively been reported, information on LMCT excited state dynamics and reactivity remains relatively scarce. It is important to note that the reversal of the charge transfer direction implies a spin-allowed ^{2}LMCT → ^{2}GS decay in iron(III) LMCT chromophores,[37] while typical MLCT chromophores are characterized by a spin-forbidden ^{3}MLCT → ^{1}GS decay. Nevertheless, this scheme may change

10.1002/chem.202200269

depending on ligand and oxidation state and, evidently, the ion's spin state.

Consequently, we sought to study the excited state dynamics of a carbene-phenolate iron complex, which we had reported in 2020 (Figure 1).[38] We had isolated this [Fe(^{NHC}OCO)$_2$] complex in three isostructural redox states, namely [**Fe^{III}(OCO)$_2$**]$^-$ (**1**) [**Fe^{IV}(OCO)$_2$**] (**2**) and [**Fe^{IV}(OCO)$_2$**]$^+$ (**3**), which thus serves as an ideal example to study the effect of the metal's redox state as well as ligand-non-innocence.

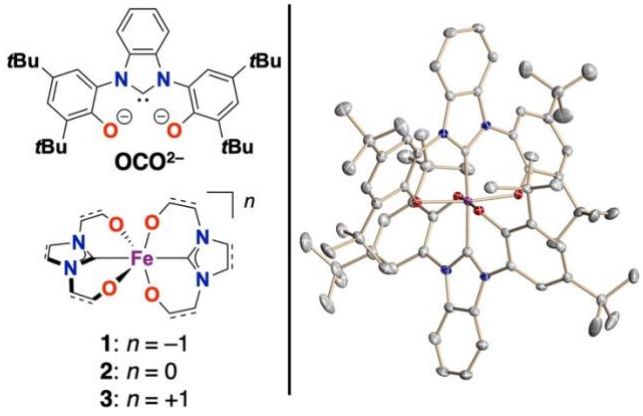

Figure 1. Left: Drawing of the NHC-anchored, dianionic OCO pincer ligand (top) and schematic representation of the iron NHC/bis-phenolate complexes discussed herein (bottom). Right: Solid-state molecular representation of **1** in crystals of [K(18c6)(THF)$_2$][Fe(^{NHC}OCO)$_2$)]·1.5 THF.[38] H atoms, the counter ion, and co-crystallized solvent molecules are omitted for clarity; thermal ellipsoids are shown at the 50% probability level.

Results and Discussion

None of the iron complexes showed room temperature luminescence in toluene or dichloromethane solutions under 300–700 nm light excitation. This is indicative for a fast deactivation of the excited states, thus requiring ultrafast, time-resolved methods to understand their photophysical properties.

Femto-Second Transient Absorption Spectroscopy (fsTAS) of 1. We started with fsTAS experiments of **1** using 20000 cm^{-1} (500 nm) excitation at room temperature in toluene (Figures 2 and S1, and Table S1; see Figures S2–S6 for excitation at 26800 cm^{-1}). Figure S1 shows the differential spectra at selected time delays, and the inverted ground state absorption as a reference. Ground state bleachings around 20000 cm^{-1} dominate the differential spectra at short time delays, which are accompanied by an NIR photoinduced absorption that peaks below 7000 cm^{-1}. Target analysis reveals two exponential processes, with lifetimes of 0.2 and 7.0 ps (Figure 2). The first excited state includes a minimum at 20000 cm^{-1} and positive signals in the NIR with a maximum below 8000 cm^{-1}. In the second excited state, photoinduced absorptions are centered at 15000 cm^{-1} and the NIR range of the spectrum is silent.

Band Assignment in Transient Spectra of 1. Time absorption changes in the NIR region during the first picosecond (Figure 2, top right panel) indicate a drastic change in the electronic configuration. We ascribe the NIR photoinduced absorptions in the first excited state to photo-induced intervalence charge transfer (PIIVCT) bands,[39,40] involving the {(OCO$^-$)(OCO^{2-})} mixed valence core. This band in **1*** originates from a {Fe^{II}(OCO$^-$)(OCO^{2-})} electronic configuration, and is the excited state equivalent to the ground state IVCT band[41,42] (GSIVCT) observed at 8900 cm^{-1} in **3** with a {Fe^{IV}(OCO$^-$)(OCO^{2-})} electronic configuration (*vide infra*).[38] In these systems, ligand-centered IVCT interactions between (OCO$^-$) and (OCO^{2-}) are probably supported by a superexchange mechanism. Thus, the iron ion can be understood as a bridge that promotes electronic coupling between the redox-active ligands.[43] This is consistent with slight energy differences between PIIVCT (< 8000 cm^{-1}) and GSIVCT (8900 cm^{-1}), both mediated by iron ions, yet in different oxidation states. Furthermore, since the formation of a {(OCO$^-$)(OCO^{2-})} mixed valence core requires a LMCT transition in **1**, the PIIVCT band is a spectroscopic hallmark of the ^{2}LMCT state.

The absence of any NIR photoinduced absorptions in the second excited state suggests the absence of mixed valency. Therefore, LMCT character seems unlikely for this excited state, which must be rather MC. Indeed, quartet and sextet MC excited states were calculated to lie 0.3–0.4 eV above the ground state in **1** (*vide infra*), supporting our assignment as a ^{4,6}MC state.[38] These observations imply that the (OCO) ligand framework is, on the contrary to borate-anchored all-carbene ligands, as in [Fe^{III}(PhB(Im^{Me})$_3$)$_2$]$^+$,[26] not a sufficiently strong donor to prevent the population of excited MC states in the +III redox state of iron.

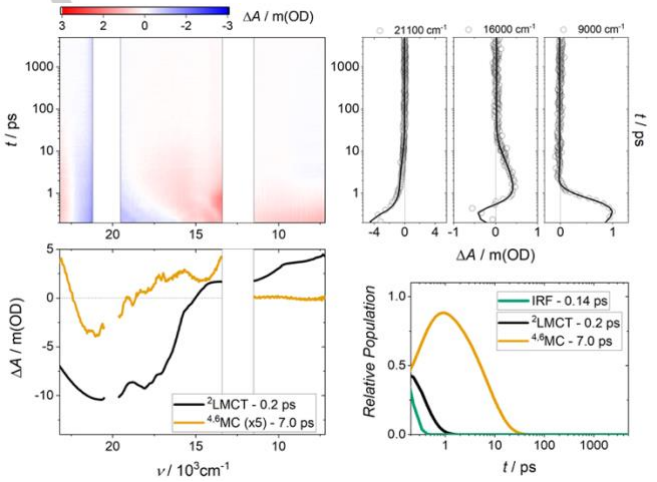

Figure 2. Differential absorption 3D map obtained from fsTAS with 20000 cm^{-1} (500 nm) excitation of **1** in toluene at room temperature (top left). Species associated differential spectra of **^{2}LMCT** and **^{4,6}MC** (bottom left). Differential absorption kinetic traces at 21100, 18300 and 7100 cm^{-1} (top right), and relative populations of **^{2}LMCT** and **^{4,6}MC** (bottom right). IRF: Instrument Response Function.

Femto-Second Transient Absorption Spectroscopy of 2. Next, we studied the fsTAS of **2**, using 26800 cm^{-1} (387 nm) excitation in toluene at room temperature (Figures 3 and S7; see Figures S8–S12 and Table S1 for the 20000 or 14400 cm^{-1} excitations, which afforded consistent results). Figure S7 shows the differential spectra at selected time delays, and the inverted ground state absorption as a reference. Upon photon absorption, positive signals at 18000 cm^{-1} and below 10000 cm^{-1} appear, together with ground state bleachings at 20000 and 14900 cm^{-1}. In the first ten picoseconds, the NIR signal shifts to higher

10.1002/chem.202200269

energies, while the rest of the differential spectrum decays without significant changes. Differential spectra at long time delays are governed by solvent related signals (Figure S6 and S13). The kinetic traces at 21100, 18300 and 7100 cm^{-1} (Figure 3, top right panel) suggest that two exponential processes and an infinite offset are required to fit the data. Indeed, target analysis reveals two exponential processes with lifetimes of 1.0 and 11.8 ps (Fig. 3, bottom left; Table S1). The applied fitting model considers two parallel pathways: First, the infinite component corresponding to the background signal of the solvent, and, second, two excited states of **2** that decay sequentially (Figure 3, bottom right panel).

Band Assignment in Transient Spectra of 2. The differential spectrum associated with the first excited state shows positive signals between 17000 and 19000 cm^{-1} as well as in the NIR region at 8000 cm^{-1}, together with ground state bleachings at 20000 and 14900 cm^{-1}. The intense NIR signals are ascribed to PIIVCT transitions within a {$(OCO^{-})(OCO^{2-})$} mixed valent ligand system. Moreover, the differential spectral profile of **2*** from fsTAS is remarkably similar to the combination of the differential reductive (Fe(IV) → Fe(III)) and differential oxidative (OCO^{2-} → OCO^{-}) spectra (Figure 4). These are obtained by subtracting the ground state absorptions of **1** minus the absorptions of **2** to mimic reduction, and subtracting absorptions of **3** minus absorptions of **2** to mimic oxidation (Figure 4). In detail, a positive signal around 18000 cm^{-1} is expected for a transition relating to an Fe(IV) → Fe(III) reduction, whereas a positive signal around 8600 cm^{-1} appears due to OCO^{2-} → OCO^{-} oxidation. Consequently, we understand this state as a vibrationally hot {$Fe^{III}(OCO^{-})(OCO^{2-})$} ligand-to-metal charge transfer (hot-^{3}LMCT state; Figure 3).

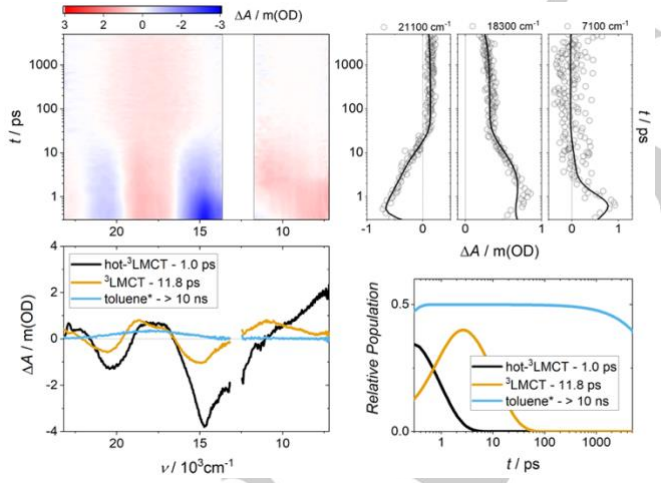

Figure 3. Differential absorption 3D map obtained from fsTAS with 26800 cm^{-1} (387 nm) excitation of **2** in toluene at room temperature (top left). Species associated differential spectra of **hot-^{3}LMCT**, **^{3}LMCT** and the solvent component (bottom left). Differential absorption kinetic traces at 21100, 18300 and 7100 cm^{-1} (top right), and relative populations of **hot-^{3}LMCT**, **^{3}LMCT** and the solvent component (bottom right).

hot-^{3}LMCT decays within 1.0 ps to a second excited state, whose differential spectrum is similar, yet with the NIR band shifted to higher energy around 11000 cm^{-1} and with reduced intensity. Thus, it is also assigned as a {$Fe^{III}(OCO^{-})(OCO^{2-})$} ^{3}LMCT state (Figure 3). The energy shift of the PIIVCT band in the excited decay cascade of **2*** is larger than 3000 cm^{-1}, which is too large to be due only to vibrational cooling within a single potential energy surface minimum. Accordingly, we believe that this process represents a vibrational relaxation with a concomitant change in the electronic configuration within the ^{3}LMCT manifold, where the excited electron occupies different orbitals of the transient Fe(III) ion. Decay to the ground state occurs within 11.8 ps, which is consistent with the absence of room temperature luminescence. Arguably, this is a consequence of intersystem crossing to MC excited states associated with the octahedral $^1T_2$ or ^{5}E states, whose lifetimes are shorter than their feeding processes; thus, preventing enough population to be detectable.

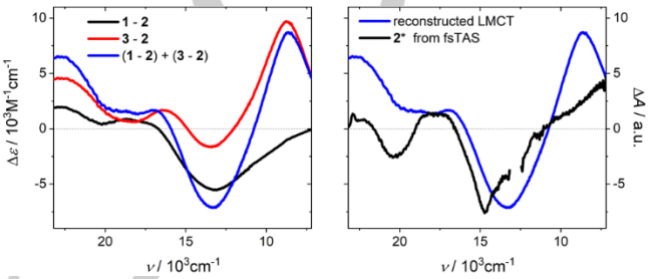

Figure 4. Left: Differential spectra upon metal-centered reduction (black) and ligand-based oxidation (red), and their additive combination (blue). Right: Reconstructed differential spectrum of the LMCT state (blue) and differential spectrum of **2*** from fsTAS (black).

Femto-Second Transient Absorption Spectroscopy of 3. Finally, we turned our attention to the fsTAS of **3**, using 26800 cm^{-1} excitation at room temperature (Fig. 5, top left; Fig. S14). Due to the low solubility of the cationic complex in toluene, we chose THF as a solvent. Besides ground state bleachings at 15000 and 9000 cm^{-1}, a photoinduced absorption at 18000 cm^{-1} is observed. The signals decay to zero within tens of picoseconds. The kinetic traces at 21000, 18300 and 7100 cm^{-1} suggest the evolution of two exponential processes (Figure 5, top right panel). Similar to **2**, target analysis of the data of **3** reveals the presence of two excited states, with lifetimes of 0.7 and 10.2 ps, respectively.

Band Assignment in Transient Spectra of 3. The associated differential spectra, which are remarkably similar one to the other, are shown at the bottom, left, in Figure 5. Intriguingly, they also are very similar in the visible range to the differential spectra recorded for **2**, whereas differences in the NIR are discernible. These observations are interpreted by population of ^{4}LMCT states for **3***, where the remaining OCO^{2-} ligand has also transferred an electron to the iron(IV). Hence, these excited states can be understood as an {$Fe^{III}(OCO^{-})_2$} electronic configuration, and are the one electron oxidized analogs of {$Fe^{III}(OCO^{-})(OCO^{2-})$} in **2***. This is supported by a positive signal at 18000 cm^{-1}, indicating a transient Fe(III) population. Since the (OCO^{-}) ligand moieties in the ^{4}LMCT state do not share a mixed valence redox state, the ground state IVCT absorption of **3** bleaches in the NIR differential spectrum of the ^{4}LMCT state. Independent fsTAS experiments on **3**, using 20000 or 14400 cm^{-1} excitation, afford similar results (Figures S15–S19, Table S1). Notably, although the oxidation state of the iron ion in the ground state of **3** is challenging to

10.1002/chem.202200269

assess – intrinsically linked to a high degree of covalency – fsTAS reveals that, in the excited state, it unambiguously behaves as an iron(IV) complex with populated, transient iron(III) LMCT states.

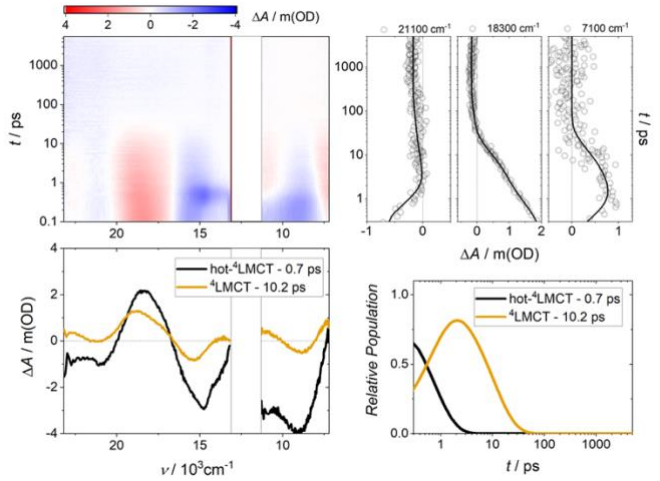

Figure 5. Differential absorption 3D map obtained from fsTAS with 26800 cm^{-1} (387 nm) excitation of **3** in THF at room temperature (top left). Species associated differential spectra of **hot-^{4}LMCT** and **^{4}LMCT**. Differential absorption kinetic traces at 21100, 18300 and 7100 cm^{-1} (top right), and relative populations of **hot-^{4}LMCT** and **^{4}LMCT**.

Discussion of Jablonski Diagrams

The Jablonski diagram in Figure 6 summarizes our observations (see the Supporting Information for further details). The excited state dynamics of both iron(IV) species **2** and **3** are not significantly influenced by ligand-centered oxidation. In both cases, LMCT lifetimes are similar to those found in the only documented iron(IV) complex to the best of our knowledge hitherto studied in this context, which refers to the strong tris-carbene donor chelate, namely phenyl[tris(3-methylimidazol-1-ylidene)]borate $(PhB(Im^{Me})_3)^-$.[44] This illustrates the difficulties in destabilizing MC states in iron(IV) complexes.

Noteworthy, classic MLCT chromophores do not exhibit particularly active NIR regions in transient absorption spectroscopy. This is related to the very weak ground-state IVCT absorptions of their reduced forms. For example, in $[Ru(bpy)_2(bpy^-)]^+$, the reduced form of $[Ru(bpy)_3]^{2+}$, the IVCT extinction coefficient is around 100 M^{-1} cm^{-1},[45] and therefore the MLCT excited states of $[Ru(bpy)_3]^{2+}$ are NIR silent. Exceptions include intra-ligand transitions in complexes of 4,4'-dicarboxy-functionalized bpy ligands,[46,47] or bimetallic compounds with significant electronic communication.[39,48–50] As far as we are aware of, there is only one report concerning a weak inter-ligand PIIVCT within the MLCT manifold of $[Os(phen)_3]^{2+}$.[51] In stark contrast, **3** displays an intense IVCT band in the ground state with an extinction coefficient of 8600 M^{-1} cm^{-1},[38] which translates to a high NIR activity in the LMCT excited states of **1** and **2**. We believe that these differences are rooted in the degree of metal-ligand covalency. The Fe-O bonds in these high-valent iron complexes display substantial covalency (*cf.* Fig. S20-22), which favors iron-mediated ligand-ligand electronic coupling.[52] This leads to mixing of ligand-based orbitals and intense IVCT bands. On the contrary, the covalent character of the Ru-N bonds in $[Ru(bpy)_3]^{2+}$ is low, which results in poor mixing of bpy-based orbitals and hence weak IVCT bands.

Calculations

In order to further substantiate the complexes' intricate electronic structure and excited energy landscape, state averaged CASSCF/NEVPT2 calculations were performed. In sight of the size of the molecules as well as the arguably required active space, these calculations turned out to be challenging. Also, results from various active spaces, such as CASSCF(12,9) *vs.* CASSCF(12,13) *vs.* CASSCF(12,15), in case of **2**, did not afford consistent results regarding the energetic ordering of the ligand- and MC states. That said, the computational results are in agreement with the spectroscopic findings reported herein and in the previous work: According to CASSCF(13,13)/NEVPT2, compound **1** is predicted to have a doublet ground state with low-lying sextet (DE^{Se1} = 0.24 eV), quartet- (DE^{Q1} = 0.35 eV; DE^{Q2} = 0.36 eV) and doublet (DE^{D1} = 0.26 eV; DE^{D2} = 0.27 eV) excited states. These excited states relate to metal-centered d-d transitions (Figure S20, Tables S2-S6). Excitation at 500 nm (2.48 eV) is likely to give either DE^{D3} = 2.16 eV or $DE^{D4,D5}$ = 2.19 eV, which are also MC states without mixed-valency of the ligand. The triplet ground state in **2** is heavily multiconfigurational according to CASSCF(12,9) calculations, yet features a strong weight (c = 0.22) of the configuration relating to a d^4-configured metal center (Figure S21, Tables S7-S8). Many low-energy LMCT states are found on the singlet, triplet and quintet potential energy surfaces. These include the T20 excited state calculated at 1100 cm^{-1} (899 nm, 1.10 eV), which is accessible *via* an intense transition (f^{osc} = 0.29) from the T0 ground state. Eventually, **3** is predicted to clearly feature oxidized, mixed-valent ligands (Figure S22, Tables S9-S11). According to CASSCF(9,9)/NEVPT2, the doublet and quartet ground states are close in energy (DE = 0.1 eV). Again, a plethora of low-energy excited states (*e.g.*, DE^{D1} = +0.10 eV; DE^{Q1} = +0.16 eV) is found, which renders the assignment of transitions challenging. However, excitation at 695 nm may populate the Q3 state (DE^{Q3} = +0.30 eV), where the lead configuration (c = 0.15) is associated with two oxidized ligands, *i.e.* an LMCT. The same is true for the Q1 state (DE^{Q2} = +0.26 eV; c = 0.20).

10.1002/chem.202200269

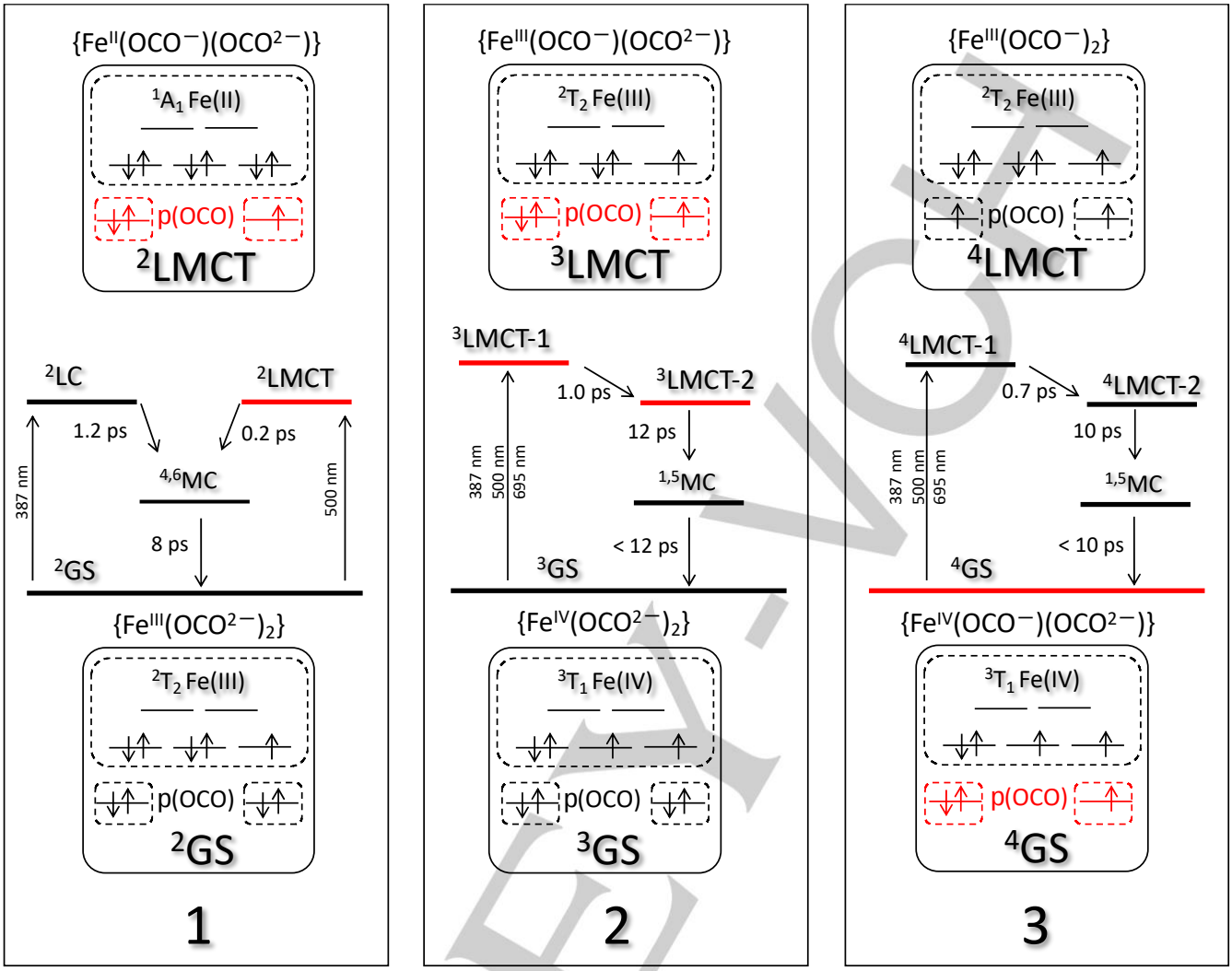

Figure 6. Jablonski diagrams and schematic electronic configurations of **1**, **2** and **3** with their corresponding LMCT excited states. Designation of MC states and electronic configurations of iron ions are approximated in octahedral symmetry. Excited states with intervalence charge transfer activity, and orbitals of ligand centered mixed valency, are highlighted in red. See the Supporting Information for details regarding the designation of the excited states and electronic configurations.

Conclusion

LMCT excited states in an iron complex in three oxidation states with a mixed phenolate/*N*-heterocyclic carbene ligand have been studied using femto-second transient absorption spectroscopy (fsTAS). All complexes display intense ground state LMCT absorptions. The iron(III) complex' LMCT lifetime is in the sub-picosecond time scale due to efficient population of low-energy MC excited states. LMCT lifetimes of iron(IV) species are longer, thus emphasizing the importance of covalency, yet still too short for bimolecular or long-range photoinduced reactivity. These observations indicate that carbene-anchored bis-phenolate pincer ligand scaffolds are not sufficiently strong donors to prevent the population of MC states in high-valent iron complexes, which are responsible for fast non-radiative deactivation. Whereas CASSCF/NEVPT2 calculations struggle to accurately reproduce the spectroscopic findings, they are in general agreement with the previous experiments[38] and the spectroscopic results reported herein. We thus propose PIIVCT bands, which occur in an energy range that is usually silent, as a general and convenient fingerprint in inorganic photochemistry with LMCT chromophores.

Experimental Section

1, 2 and **3** were prepared following a reported procedure.[38] UV-visible spectra were recorded with an AvaSpec 2048 spectrometer. Emission spectroscopy was performed on a Fluoromax 3 spectrometer from Horiba Yovin Yvon. Ultrafast transient absorption experiments were conducted using an amplified Ti:sapphire fs laser system (Clark MXR CPA2101 and 2110, 1kHz, FWHM = 150 fs, λ^{exc} = 387, 500 and 695 nm, 300-700 nJ per pulse) with TA pump / probe Helios detection system from Ultrafast Systems. White light was generated focusing a fraction of the fundamental 775 nm output onto a 2 mm sapphire disk (~430−760 nm) or a 1 cm sapphire disk (~800−1600 nm). A magic angle configuration between the

pump and the probe beams was employed to avoid rotational dynamics. Excitation pulses were generated by frequency doubling or a NOPA. Bandpass filters with ± 5 or ± 10 nm were used to ensure low spectral width and to exclude 775 nm photons. Typical excitation spot areas are around 500 mm and ensured to be larger than those of the probe beam. All measurements were conducted in a 2 mm quartz cuvette under argon atmosphere and continuous magnetic stirring, using solutions with absorbances of 0.5-0.7. Omitted regions of the experimental spectra are due to scattering of residual 775 nm and pump wavelength photons. To analyze transient absorption data, we used a suggested procedure.[53] We start with SVD and global analysis, using an all-sequential decay model that provides evolution associated spectra of potentially intervening species, to determine the number of decaying species that participate in the decay cascade. However, this doesn't necessary yield differential spectra with genuine physicochemical meaning. Afterwards, a target analysis is applied, using specific target models that result in species associated spectra with true physicochemical meaning. Obtained data were treated by SVD, global and target analyses using the R- package TIMP and GloTarAn.[53–55]

Acknowledgements

A.C. is associated to ALN and a member of the research staff of CONICET. A.C. thanks Dirk M. Guldi for providing access to transient absorption facilities. D.M. thanks the RRZ Erlangen for computational resources.

Keywords: Photoinduced Mixed Valence • Iron NHC Complexes • Iron Phenolate Complexes • Ultrafast Spectroscopy • LMCT Excited State

[1] L. Armelao, S. Quici, F. Barigelletti, G. Accorsi, G. Bottaro, M. Cavazzini, E. Tondello, *Coord. Chem. Rev.* **2010**, *254*, 487–505.
[2] R. D. Dill, R. I. Portillo, S. G. Shepard, M. P. Shores, A. K. Rappé, N. H. Damrauer, *Inorg. Chem.* **2020**, *59*, 14706–14715.
[3] M. Dorn, J. Kalmbach, P. Boden, A. Päpcke, S. Gómez, C. Förster, F. Kuczelinis, L. M. Carrella, L. A. Büldt, N. H. Bings, E. Rentschler, S. Lochbrunner, L. González, M. Gerhards, M. Seitz, K. Heinze, *J. Am. Chem. Soc.* **2020**, *142*, 7947–7955.
[4] J. R. Jiménez, M. Poncet, B. Doistau, C. Besnard, C. Piguet, *Dalton Trans.* **2020**, *49*, 13528–13532.
[5] S. Treiling, C. Wang, C. Förster, F. Reichenauer, J. Kalmbach, P. Boden, J. P. Harris, L. M. Carrella, E. Rentschler, U. Resch-Genger, C. Reber, M. Seitz, M. Gerhards, K. Heinze, *Angew. Chem.Int.Ed.* **2019**, *58*, 18075–18085; *Angew. Chem.* **2019**, 131, 18243-18253.
[6] L. A. Büldt, X. Guo, R. Vogel, A. Prescimone, O. S. Wenger, *J. Am. Chem. Soc.* **2017**, *139*, 985–992.
[7] J. P. Harris, C. Reber, H. E. Colmer, T. A. Jackson, A. P. Forshaw, J. M. Smith, R. A. Kinney, J. Telser, *Can. J. Chem.* **2017**, *95*, 547–552.
[8] S. Kaufhold, K. Wärnmark, *Catalysts* **2020**, *10*, 132–163.
[9] L. Lindh, P. Chábera, N. W. Rosemann, J. Uhlig, K. Wärnmark, A. Yartsev, V. Sundström, P. Persson, *Catalysts* **2020**, *10*, 315–345.
[10] B. C. Paulus, S. L. Adelman, L. L. L. Jamula, J. K. K. McCusker, *Nature* **2020**, *582*, 214–218.
[11] P. Chábera, Y. Liu, O. Prakash, E. Thyrhaug, A. El Nahhas, A. Honarfar, S. Essén, L. A. Fredin, T. C. B. Harlang, K. S. Kjær, K. Handrup, F. Ericson, H. Tatsuno, K. Morgan, J. Schnadt, L. Häggström, T. Ericsson, A. Sobkowiak, S. Lidin, P. Huang, S. Styring, J. Uhlig, J. Bendix, R. Lomoth, V. Sundström, P. Persson, K. Wärnmark, *Nature* **2017**, *543*, 695–699.
[12] C. B. Larsen, J. D. Braun, I. B. Lozada, K. Kunnus, E. Biasin, C. Kolodziej, C. Burda, A. A. Cordones, K. J. Gaffney, D. E. Herbert, *J. Am. Chem. Soc.* **2021**, *143*, 20645–20656.
[13] A. K. Pal, C. Li, G. S. Hanan, E. Zysman-Colman, *Angew. Chemie Int. Ed.* **2018**, *57*, 8027–8031; *Angew. Chem.* **2018**, *130*, 8159–8163.
[14] M. Iwamura, S. Takeuchi, T. Tahara, *Acc. Chem. Res.* **2015**, *48*, 782–791.
[15] R. Hamze, J. L. Peltier, D. Sylvinson, M. Jung, J. Cardenas, R. Haiges, M. Soleilhavoup, R. Jazzar, P. I. Djurovich, G. Bertrand, M. E. Thompson, *Science* **2019**, *363*, 601–606.
[16] D. Di, A. S. Romanov, L. Yang, J. M. Richter, J. P. H. Rivett, S. Jones, T. H. Thomas, M. Abdi Jalebi, R. H. Friend, M. Linnolahti, M. Bochmann, D. Credgington, *Science* **2017**, *356*, 159–163.
[17] Y. Zhang, T. S. Lee, J. M. Favale, D. C. Leary, J. L. Petersen, G. D. Scholes, F. N. Castellano, C. Milsmann, *Nat. Chem.* **2020**, *12*, 345–352.
[18] P. Pinter, C. M. Schüßlbauer, F. A. Watt, N. Dickmann, R. Herbst-Irmer, B. Morgenstern, A. Grünwald, T. Ullrich, M. Zimmer, S. Hohloch, D. M. Guldi, D. Munz, *Chem. Sci.* **2021**, *12*, 7401–7410.
[19] O. Back, C. Förster, T. Basché, K. Heinze, *Chem. - A Eur. J.* **2019**, *25*, 6542–6552.
[20] C. Förster, K. Heinze, *Chem. Soc. Rev.* **2020**, *49*, 1057–1070.
[21] C. Wegeberg, O. S. Wenger, *JACS Au* **2021**, *1*, 1860–1876.
[22] M. S. Lazorski, F. N. Castellano, *Polyhedron* **2014**, *82*, 57–70.
[23] T. C. B. Harlang, Y. Liu, O. Gordivska, L. A. Fredin, C. S. Ponseca, P. Huang, P. Chábera, K. S. Kjaer, H. Mateos, J. Uhlig, R. Lomoth, R. Wallenberg, S. Styring, P. Persson, V. Sundström, K. Wärnmark, *Nat. Chem.* **2015**, *7*, 883–889.
[24] Y. Liu, S. C. Yiu, C. L. Ho, W. Y. Wong, *Coord. Chem. Rev.* **2018**, *375*, 514–557.
[25] J. D. Braun, I. B. Lozada, C. Kolodziej, C. Burda, K. M. E. Newman, J. van Lierop, R. L. Davis, D. E. Herbert, *Nat. Chem.* **2019**, *11*, 1144–1150.
[26] K. S. Kjær, N. Kaul, O. Prakash, P. Chábera, N. W. Rosemann, A. Honarfar, O. Gordivska, L. A. Fredin, K. E. Bergquist, L. Häggström, T. Ericsson, L. Lindh, A. Yartsev, S. Styring, P. Huang, J. Uhlig, J. Bendix, D. Strand, V. Sundström, P. Persson, R. Lomoth, K. Wärnmark, *Science* **2019**, *363*, 249–253.
[27] M. Bauer, J. Steube, P. Ayle, O. Bokareva, T. Reuter, S. Demeshko, R. Schoch, S. Hohloch, F. Meyer, K. Heinze, S. Lochbrunner, *Res. Sq.* **2020**, 1–19.
[28] W. Leis, M. A. Argüello Cordero, S. Lochbrunner, H. Schubert, A. Berkefeld, *J. Am. Chem. Soc.* **2022**, *144*, 1169–1173.
[29] O. S. Wenger, *Chem. - A Eur. J.* **2019**, *25*, 6043–6052.
[30] J. K. McCusker, *Science* **2019**, *363*, 484–488.
[31] C. Vogel, F. W. Heinemann, J. Sutter, C. Anthon, K. Meyer, *Angew. Chem.Int.Ed.* **2008**, *47*, 2681–2684; *Angew. Chem.* **2008**, *120*, 2721–2724.
[32] J. J. Scepaniak, M. D. Fulton, R. P. Bontchev, E. N. Duesler, M. L. Kirk, J. M. Smith, *J. Am. Chem. Soc.* **2008**, *130*, 10515–10517.
[33] T. A. Betley, J. C. Peters, *J. Am. Chem. Soc.* **2004**, *126*, 6252–6254.
[34] J. J. Scepaniak, C. S. Vogel, M. M. Khusniyarov, F. W. Heinemann, K. Meyer, J. M. Smith, *Science* **2011**, *331*, 1049–1052.
[35] J. L. Martinez, S. A. Lutz, H. Yang, J. Xie, J. Telser, B. M. Hoffman, V. Carta, M. Pink, Y. Losovyj, J. M. Smith, *Science* **2020**, *370*, 356–359.
[36] M. Keilwerth, L. Grunwald, W. Mao, F. W. Heinemann, J. Sutter, E. Bill, K. Meyer, *J. Am. Chem. Soc.* **2021**, *143*, 1458–1465.
[37] P. Chábera, L. Lindh, N. W. Rosemann, O. Prakash, J. Uhlig, A. Yartsev, K. Wärnmark, V. Sundström, P. Persson, *Coord. Chem. Rev.* **2021**, *426*, 213517.
[38] L. Gravogl, F. W. Heinemann, D. Munz, K. Meyer, *Inorg. Chem.* **2020**, *59*, 5632–5645.
[39] B. M. Aramburu-Trošelj, P. S. Oviedo, I. Ramírez-Wierzbicki, L. M. Baraldo, A. Cadranel, *Chem. Commun.* **2019**, *55*, 7659–7662.
[40] C. Lambert, R. Wagener, J. H. Klein, G. Grelaud, M. Moos, A. Schmiedel, M. Holzapfel, T. Bruhn, *Chem. Commun.* **2014**, *50*, 11350–11353.
[41] D. M. D'Alessandro, F. R. Keene, *Chem. Rev.* **2006**, *106*, 2270–2298.
[42] J. Hankache, O. S. Wenger, *Chem. Rev.* **2011**, *111*, 5138–5178.
[43] A. Arrigo, A. Santoro, M. T. Indelli, M. Natali, F. Scandola, S. Campagna, *Phys. Chem. Chem. Phys.* **2014**, *16*, 818–826.
[44] O. Prakash, P. Chábera, N. W. Rosemann, P. Huang, L. Häggström, T. Ericsson, D. Strand, P. Persson, J. Bendix, R. Lomoth, K. Wärnmark, *Chem. - A Eur. J.* **2020**, *26*, 12728–12732.
[45] G. A. Heath, L. J. Yellowlees, P. S. Braterman, *Chem. Phys. Lett.* **1982**, *92*, 646–648.
[46] C. M. Elliott, E. J. Hershenhart, *J. Am. Chem. Soc.* **1982**, *104*, 7519–7526.
[47] M. Murai, A. Furube, M. Yanagida, K. Hara, R. Katoh, *Chem. Phys. Lett.* **2006**, *423*, 417–421.
[48] B. M. Aramburu-Trošelj, P. S. Oviedo, G. E. Pieslinger, J. H. Hodak, L. M. Baraldo, D. M. Guldi, A. Cadranel, *Inorg. Chem.* **2019**, *58*, 10898–10904.
[49] B. M. Aramburu-Trošelj, I. Ramírez-Wierzbicki, F. Scarcasale, P. S. Oviedo, L. M. Baraldo, A. Cadranel, *J. Phys. Chem. Lett.* **2020**, *11*, 8399–8405.
[50] P. S. Oviedo, L. M. Baraldo, A. Cadranel, *Proc. Natl. Acad. Sci.* **2021**, *118*, e2018521118.
[51] D. M. Dattelbaum, E. M. Kober, J. M. Papanikolas, T. J. Meyer, *Chem. Phys.* **2006**, *326*, 71–78.
[52] R. G. Hadt, S. I. Gorelsky, E. I. Solomon, *J. Am. Chem. Soc.* **2014**, *136*, 15034–15045.
[53] I. H. M. Van Stokkum, D. S. Larsen, R. Van Grondelle, *Biochim. Biophys. Acta - Bioenerg.* **2004**, *1657*, 82–104.
[54] J. J. Snellenburg, S. Laptenok, R. Seger, K. M. Mullen, I. H. M. van

Stokkum, *J. Stat. Softw.* **2012**, *49*, 1–22.
[55] K. M. Mullen, I. H. M. Van Stokkum, *J. Stat. Softw.* **2007**, *18*, 1–46.

10.1002/chem.202200269